Methane Conversion to Aromatics on Mo/H-ZSM5: Structure of Molybdenum Species in Working Catalysts

Weiping Ding,[†] Senzi Li, George D Meitzner,[‡] and Enrique Iglesia*

Materials Sciences Division, E. O. Lawrence Berkeley National Laboratory, and Department of Chemical Engineering, University of California at Berkeley, Berkeley, California 94720

Received: August 24, 2000; In Final Form: October 27, 2000

The structure and density of Mo species in Mo/H−ZSM5 during catalytic CH_4 reactions was investigated using in-situ X-ray absorption spectroscopy (XAS), temperature-programmed oxidation after reaction, and the isotopic exchange of D_2 with OH groups in H−ZSM5 before and after CH_4 reactions. These methods reveal that CH_4 reactions cause exchanged $Mo_2O_5^{2+}$ dimers, formed from physical mixtures of MoO_3 and H−ZSM5, to reduce and carburize to form small (0.6−1 nm) MoC_x clusters with the concurrent regeneration of the bridging OH groups that were initially replaced by Mo oxo dimers during exchange. In this manner, catalytically inactive Mo oxo species activate in contact with CH_4 to form the two sites required for the conversion of CH_4 to aromatics: MoC_x for C−H bond activation and initial C−C bond formation and acid sites for oligomerization and cyclization of C_{2+} hydrocarbons to form stable aromatics. These MoC_x clusters resist agglomeration during methane reactions at 950 K for > 10 h. The Brönsted acid sites formed during carburization and oligomerization of MoC_x species ultimately become covered with hydrogen-deficient reaction intermediates (H/C ∼ 0.2) or unreactive deposits. The highly dispersed nature of the MoC_x clusters was confirmed by detailed simulations of the XAS radial structure function and by the low temperatures required for the complete oxidation of these MoC_x species compared with bulk Mo_2C. Initial CH_4 reactions with MoO_x precursors are stoichiometric and lead first to the removal of oxygen as CO, CO_2, and H_2O and to the introduction of carbidic carbons into the reduced structures. As carbidic carbon passivates the surface, C−H bond activation reactions become catalytic by the coupling of this activation step with the removal of the resulting CH_x species to form C_2 hydrocarbons, which desorb to re-form the MoC_x sites required for C−H bond activation steps.

Introduction

The activation of CH_4 and its conversion to higher hydrocarbons remains an important challenge posing significant thermodynamic and kinetic hurdles.[1−4] The catalytic conversion of methane to aromatics via non-oxidative routes has attracted significant attention since the initial report of the selective formation of benzene at near equilibrium concentrations on Mo/H−ZSM5 [5]. Subsequently, many catalysts consisting of transition metal ions, such as Mo, W, V, Fe, and Cr, exchanged into or loaded onto various zeolites (H−ZSM5, H−ZSM11, H−ZSM8, H-beta, H−MCM41, HY, and H-mordenite) have been examined for this reaction.[6−8] Mo/H−ZSM5 remains the most attractive catalyst and several synthetic routes and zeolite sources have led to similar catalytic performance, in most cases because such materials achieve near equilibrium methane conversions with high selectivity to benzene.

The detailed mechanism of the initial C−C bond formation and of the structure of the active Mo species during catalysis remain unclear. Xu et al. speculated that heterolytic splitting of C−H bonds in CH_4 on acid sites and molybdenum carbene-like complexes are involved.[9] These molybdenum carbene complexes then dimerized to form ethylene as the first product. These authors have also suggested that the active centers consist of partially reduced molybdenum oxide species MoO_{3-x}.[10] Lin et al. proposed that the activation of methane to form CH_3 free radicals requires the synergistic involvement of MoO_x and Brönsted acid sites and that the CH_3 free radicals then dimerize in the gas phase to form ethane as the first product.[11] These early mechanistic proposals have remained speculative and lack direct experimental support. Lunsford et al., using X-ray photoelectron spectroscopy, showed that Mo_2C is present in Mo/H−ZSM5 catalysts after CH_4 reactions. They detected carbidic carbon on Mo/H−ZSM5 and showed that MoO_x species reduce to almost zero valency during reaction;[12] they also suggested that molybdenum carbide clusters within zeolite channels are involved in rate-determining C−H bond activation steps to form ethylene and H_2 as products. Solymosi et al.[13−16] explored the catalytic behavior of unsupported and supported Mo species; they concluded that Mo_2C provides the active sites for ethylene formation, and that acid sites catalyze its subsequent conversion to benzene. More recently, Lunsford et al. proposed a critical role of carbonaceous deposits in the reaction chemistry; they found that the preformation of Mo_2C without excess carbon did not eliminate the initial activation period observed with Mo(VI) precursors during methane reactions.[17]

Previously, we have shown that MoO_3 species migrate into zeolite channels and exchange with OH groups in H−ZSM5 to form $(Mo_2O_5)^{2+}$ dimers, anchored at two cation exchange sites (Scheme 1), when MoO_3/H−ZSM5 physical mixtures are heated in dry air.[18−21] These results confirmed the highly dispersed and unreduced nature of catalyst precursors. In these studies,

* To whom correspondence should be addressed. E-mail: iglesia@cchem.berkeley.edu.

[†] Permanent address: Department of Chemistry, Nanjing University, Nanjing 210093, China.

[‡] Edge Analytical Inc., 2126 Allen Blvd #3, Middleton WI 53562, USA.

10.1021/jp0030692 CCC: $20.00
Published on Web 12/21/2000

SCHEME 1. Solid Exchange of MoO_3 with OH Groups of H-ZSM5

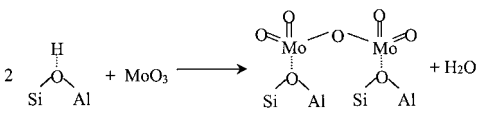

we also measured the amount of oxygen removed during methane reactions and confirmed the reduction and carburization of these materials using in situ X-ray absorption spectroscopy.[18−21] Here, we describe our additional recent results dealing with the reduction, carburization, and migration of Mo species during CH_4 reactions. Our approach includes in-situ X-ray absorption spectroscopy, temperature-programmed oxidation after reaction, and the isotopic exchange of D_2 with zeolitic OH groups in H−ZSM5 before and after activation and CH_4 reactions.

Experimental Methods

Mo/H−ZSM5 (4 wt % Mo) was prepared from physical mixtures of H−ZSM5 (Zeolyst International, Si/Al=15) and bulk MoO_3 powder (Johnson Matthey Electronics, 99.95%). Powder mixtures were ground in an agate mortar for 0.5 h, pressed into lose pellets, and crushed to 35 ∼ 60 mesh before thermal treatment. These mixtures were then treated as follows before isothermal transient reduction or reaction (ITR), isotopic D_2 exchange with OH groups, and temperature-programmed oxidation (TPO) studies:

(a) MoO_3/H−ZSM5 physical mixtures (0.2 g) were placed in a quartz cell.

(b) Samples were heated in 100 cm^3/min 20% O_2/He (Airgas, ultrahigh purity grade) at 10 K/min to 973 K and held for 0.5 h; this procedure leads to the quantitative exchange of MoO_3, predominantly as Mo oxo dimers $(Mo_2O_5)^{2+}$.[18−21]

(c) Samples were cooled in He (100 cm^3/min, Airgas, ultrahigh purity) to 950 K.

(d) The flow was switched to CH_4/Ar/He (1:1:3; 100 cm^3/min) and maintained for various periods of time. The concentration of unreacted CH_4 and of reaction products was monitored by mass spectrometry (Leybold-Inficon Transpector 1.0). Ar was used as an internal standard in order to calculate CH_4 conversion and the rate of evolution of products.

(e) Samples were then treated in 100 cm^3/min H_2/He (40%, Matheson, high purity grade) at 950 K for 2 h [hydrocarbons (CH_4, C_2H_4, C_6H_6) were no longer detected after 0.5 h] followed by He treatment for 1 h at 950 K. This procedure was used to attempt to desorb any reaction intermediates present on the surface of the catalyst during CH_4 reactions.

(f) Samples were cooled to room temperature in 100 cm^3/min He.

(g) The flow was switched to 60 cm^3/min D_2/Ar (5%, Matheson), and deuterium exchange with protium present in the sample was measured by increasing the temperature to 973 K at 10 K/min.

(h) The carrier gas was switched from D_2/Ar to H_2/He (10%) at 973 K for 10 min (D is re-exchanged back to H so that H_2O can be measured during subsequent TPO.)

(i) Samples were cooled to room temperature in 100 cm^3/min He

(j) The flow was switched to 100 cm^3/min O_2/He (40%) in order to carry out the temperature-programmed oxidation of carbonaceous deposits to CO_x and H_2O by increasing the sample temperature to 973 K at 10 K/min.

X-ray absorption spectroscopic (XAS) measurements were carried out at beamline BL2−3 in the Stanford Synchrotron Radiation Laboratory (SSRL). A Si (220) double crystal monochromator was used to obtain a monochromatic X-ray beam. The in-situ XAS cell has been described previously.[22] A physical mixture of H−ZSM5 and MoO_3 containing 4wt % Mo (24 mg; particles < 60 mesh) was placed within a quartz tube of 2 mm diameter and wall thickness < 0.1 mm. The samples were heated in flowing 20% O_2/He (2 cm^3/min) to 973 K at 10 K/min, held for 0.5 h, and then cooled to room temperature in He before XAS data were collected after the exchange process. Then, the samples were heated in He to 955 K and He was switched to CH_4/Ar (1 cm^3/min) for various periods of time. XAS data were collected on reduced-carburized samples at room temperature in flowing He.

XAS measurements were also carried out for a Mo_2C sample synthesized within the XAS cell. MoO_3 (3 mg) diluted with graphite (4 mg) was placed in the cell and heated in a 20% CH_4/H_2 (2 cm^3/min) to 1023 K at 10 K/min and held at this temperature for 0.5 h. This procedure leads to the formation of crystalline β-Mo_2C.[23]

EXAFS (Extended X-ray Absorption Fine Structure) data were analyzed using WinXas97[24] (version 1.2) and FEFF8.0.[25] The code ATOMS[26] was used to provide coordination numbers and interatomic distances from compounds with known structures (Mo, MoO_3, MoO_2, Mo_2C) for use in the cluster simulations. The k^3-weighted EXAFS was Fourier transformed in the range 0.3 ∼ 1.5 nm^{-1} and fitted in R-space to 0.8 nm, using a Mo_2C cluster of radius 0.4 nm as a starting model. A multishell fitting was used to determine interatomic distances (R), coordination numbers (CN), and energy shifts (ΔE_0).

Results and Discussion

Figure 1 shows methane conversion and product formation rates at 950 K during the initial exposure of exchanged Mo/H−ZSM5 samples to methane (step (d) in methods section). Accurate determinations of the concentrations of species in the complex product mixture were achieved using frequent calibrations of the mass fragmentation patterns of individual compounds and matrix deconvolution methods that account for overlapping mass fragments arising from the complex product mixture.[27]

After an induction period of about 150 s, methane conversion rates increased sharply and subsequently decreased with reaction time. This appears to reflect the autocatalytic nature of the reduction of Mo(VI) species, which catalyze the activation of C−H bonds in CH_4 with increasing efficiency as reduction proceeds.[28] During this induction period, the conversion of methane leads predominately to CO_2, H_2O, and CO, without the concurrent formation of hydrocarbons. This reflects the partial removal of oxygen from the Mo(VI) oxo dimers in the starting material. As the reduction proceeded, the rate of methane conversion increased and CO and H_2 became the predominant products. The amount of H_2 evolved was more than two times larger than the quantity of CO formed; this shows that some carbon was retained by the catalyst as carbidic carbon, carbon-containing reactive intermediates, or deactivating deposits. Mo(VI) species were reduced to lower valent molybdenum species during the induction period of time, and then reduced further and converted to MoC_x.

Figure 2 shows the evolution of oxygen-containing products during reduction and carburization of pure MoO_3 using a 20% CH_4/H_2 mixture at conditions that lead to the formation of β-Mo_2C.[23] Figure 2 also shows the subsequent reoxidation in 20% O_2/He mixtures (100 cm^3/min) of the Mo_2C. The reaction of MoO_3 with CH_4/H_2 takes place in two stages as reported by

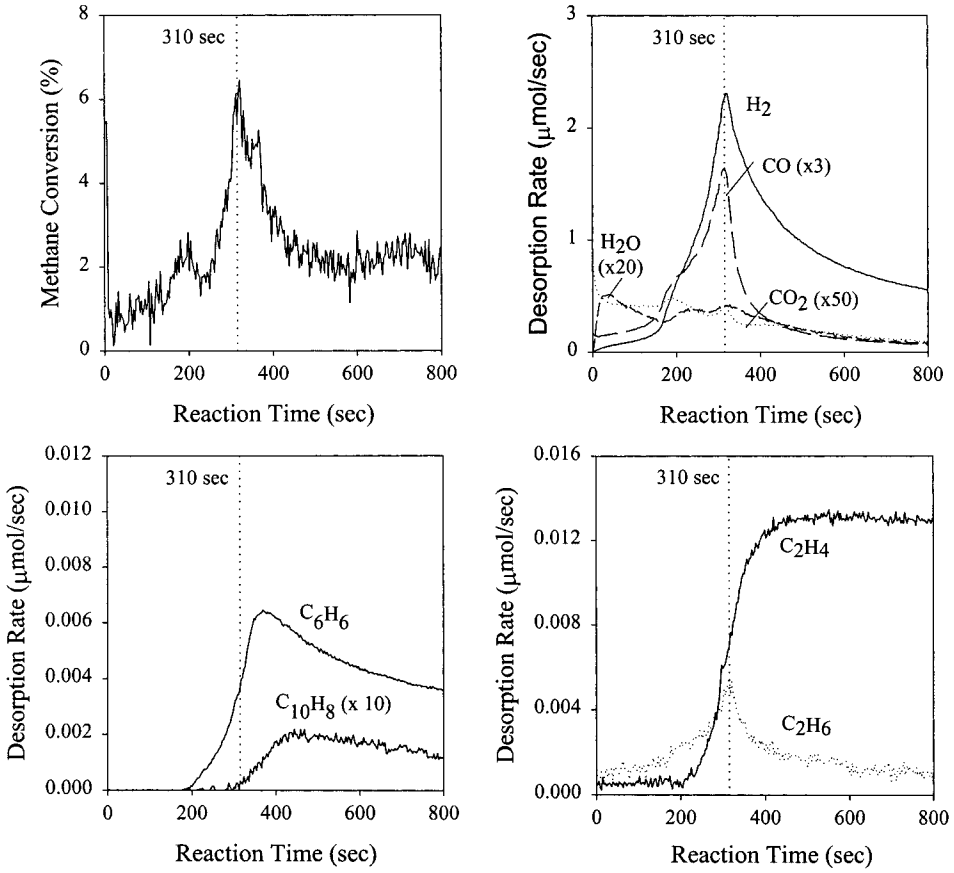

Figure 1. Transient reaction of 4 wt % Mo/H−ZSM5 with methane. (950 K, CH_4/Ar/He (1:1:1) 100 mL/min, 0.2 g Cat.)

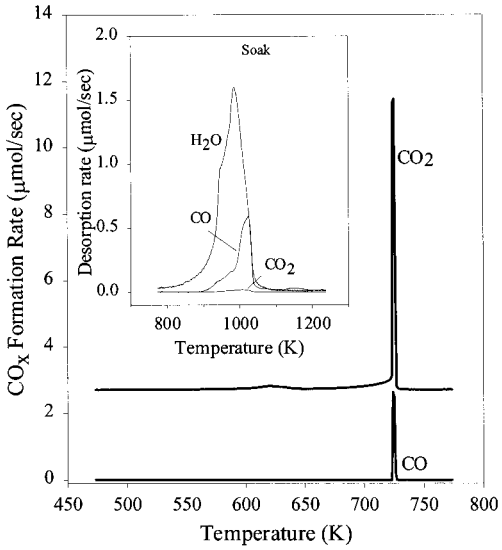

Figure 2. CO and CO_2 evolution during TPO of bulk Mo_2C. The inset shows the process of reduction and carburization of MoO_3 powder by CH_4/H_2 (1:4).

Lee et al.,[23,28−30] but the reoxidation of the Mo_2C occurs as a single fast process with the sharp evolution of CO_x at ∼725 K.

Figure 3 shows the rate of HD formation during isotopic exchange of D_2 with H-atoms after catalysts were used for methane reactions for various periods of time (step (g)) at 950 K. Exchangeable hydrogen species in these samples include OH groups (zeolitic bridged OH groups, silanols, or OH groups at extraframework Al) and hydrogen-containing carbonaceous deposits or intermediates, such as polynuclear aromatics. Maximum HD evolution rates were observed at ∼780 K and ∼610 K for H−ZSM5 and MoO_x/H−ZSM5, respectively. MoO_x species exchanged onto ZSM5 catalyze rate-determining D_2 dissociation steps during isotopic exchange more effectively than sites available in H−ZSM5. The reduction and carburization of these MoO_x species during initial contact with CH_4 at 950 K leads to even lower HD evolution peak temperatures; these temperature decreased to 475 K after CH_4 reaction for 200 s (curve *c* in Figure 3), suggesting that the MoC_x sites formed during contact of MoO_x species with CH_4 at 950 K are more active for D_2 activation than the MoO_x precursors initially present after exchange. The higher activity of MoC_x for D_2 dissociation compared with MoO_x parallels a similar trend in the catalytic behavior for hydrocarbon reactions as bulk MoO_3 converts to bulk Mo_2C. Lee et al. have reported high catalytic activity of Mo_2C loaded on γ-Al_2O_3 for hydrogenolysis of *n*-butane at 510 K.[30,31] Turnover rates for hydrogenolysis reactions on Mo_2C were high, only slightly lower than that on Ru and Os and much higher than on MoO_3.

After CH_4 reactions for ∼800 s, D_2 exchange occurs with the formation of a single HD peak at low temperatures (∼475 K). This appears to reflect the near complete reduction and carburization of the MoO_x species in the MoO_x/H−ZSM5 precursor and the formation of uniform Mo−C species. These data are in agreement with the isothermal transient data shown in Figure 1, which showed that the evolution of CO_x and H_2O during methane reactions is almost complete after about 800 s. At shorter CH_4 reaction times, the HD evolution peak at ∼475 K is more complex, apparently because incomplete conversion to Mo carbides leads to a wide range of MoO_xC_y stoichiometries and to a broad distribution of D_2 dissociation sites.

Longer CH_4 reaction times lead to the accumulation of carbon deposits and to an increase in the amount of HD evolved (shown in parentheses in Figure 3) with increasing reaction time. Thus, it appears that the surface density of OH groups or of hydrogen-

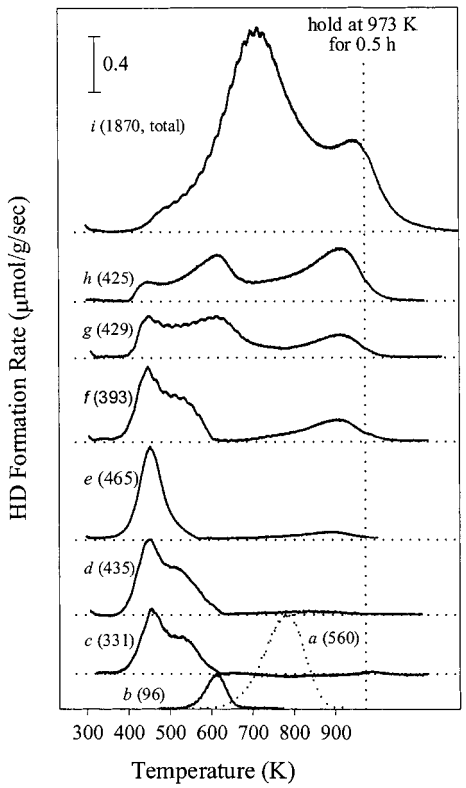

Figure 3. HD evolution during D−H exchange on 4 wt % Mo/H−ZSM5 reduced and carburized by methane. (a) H−ZSM5; (b) fresh Mo/H−ZSM5 calcined at 973 K for 0.5 h; (c) Mo/H−ZSM5 reacted with methane at 950 K for 200 s; (d) 450 s; (e) 800 s; (f) 1200 s; (g) 0.5 h; (h) 1 h; and (i) 15 h (These methane reaction times do not include the induction time.). The figures in parentheses are the molar amount of HD under peak 1 or peak 1 + peak 2 (μmol/g).

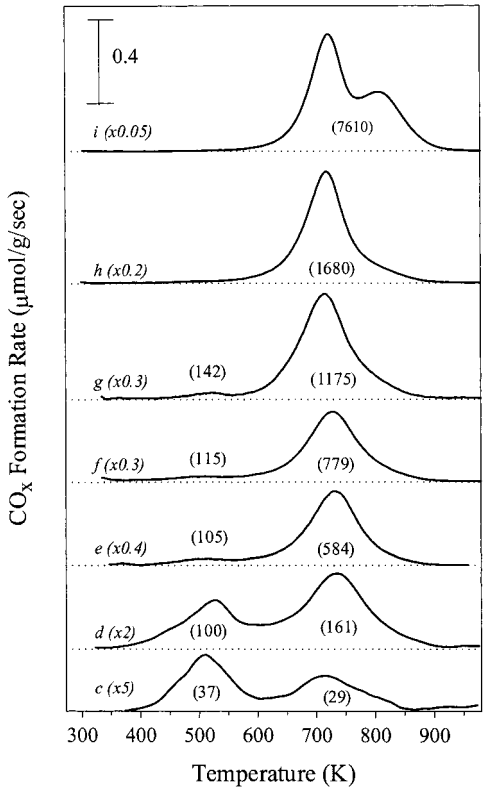

Figure 4. CO_x evolution detected in TPO on 4 wt % Mo/H−ZSM5 after methane reaction and D−H exchange. (10 K/min, 100 cm^3/min 40% O_2/He). The letters have the same meaning as in Figure 3. Figures in parentheses are amounts of CO_x under corresponding peaks (μmol/g).

containing adsorbed species increases with increasing exposure to CH_4 at 950 K. It seems reasonable to assume that OH groups account for the initial observed increase in the amount of exchangeable hydrogen atoms during methane reactions, but clearly some of the H atoms must also be present within hydrogen-containing hydrocarbon species. These conclusions are supported by the results of temperature-programmed oxidation of the reduced-carburized samples after various CH_4 reaction times (shown in Figures 4 and 5). Short methane reaction times lead to low concentrations of carbon deposits, which contain small amounts of hydrogen. The H/C ratio for carbon deposits is basically a constant 0.2, as measured by TPO for methane reactions longer than 0.3 h (cf. Figure 7). For example, the hydrogen contained in carbon deposits accounts for only ~30% of the hydrogen atoms under curve *e* in Figure 3. An increase in the number of OH groups would require that exchanged Mo species leave cation exchange sites during reduction and carburization. Methane appears to convert the isolated MoO_x dimers initially present after exchange to well-dispersed MoC_x clusters. Even if such clusters retained a positive charge in the presence of alkyl adsorbed species, the multiatomic nature of the clusters would mean that fewer exchange sites are occupied by Mo species. Therefore, acidic OH groups must form during methane reactions. In this manner, methane reactions form the two sites required for the bifunctional conversion of methane to aromatics from noncatalytic but reactive MoO_x dimers initially formed during synthesis.[8] At short contact times, these acidic OH groups are likely to account for the increase in exchangeable H-atoms; at longer times, exchanged sites are likely to adsorb instead $C_xH_yO_F$ species (O_F = framework oxygen), which act as intermediate or spectator species in the formation of higher hydrocarbons from CH_4 on Mo/H−ZSM5.

Figures 4 and 5 show the evolution of CO_x and H_2O when samples used for CH_4 reactions are treated in 40% O_2/He and the sample temperature is increased from room temperature to 973 K (procedure (j) in methods section). Three CO_x peaks were detected. A peak at ~530 K disappears at longer reaction times by merging with the peak at ~745 K. For reaction times greater than 0.3 h, a third peak appears at ~820 K. Considering the different expected reactivities of various carbon species in reactions with oxygen, we have assigned these peaks to the combustion of (1) carbidic carbon in MoC_x; (2) carbonaceous species within zeolite channels near Mo species that catalyze O_2 dissociation steps; and (3) carbon deposits distant from these Mo species. The absence of concurrent H_2O evolution during the first peak confirms its MoC_x origin. This oxidation step, however, occurs at much lower temperatures (530 K) than for bulk Mo_2C (725 K; Figure 2), suggesting that the structure and/or cluster size of MoC_x formed from MoO_x dimers in H−ZSM5 differ significantly from those in bulk Mo_2C crystallites. The formation of transition metal carbides and the reoxidation of carbides appear to be controlled by the diffusion of oxygen in or out of the bulk crystallites.[32] As a result, we infer that the small size of the MoC_x clusters in Mo/H−ZSM5 provides a much shorter diffusion path for the reoxidation of the carbide structure.

Figure 6 shows the (C/Mo) atomic ratio within the first CO_x peak as samples used in CH_4 reactions for varying periods of time were treated in O_2/He. The (C/Mo) ratio increased with increasing reaction time; it appears to approach an asymptotic value of 0.5 at long reaction times. Figure 7 shows the H/C atomic ratio obtained from the H_2O and CO_x formed during

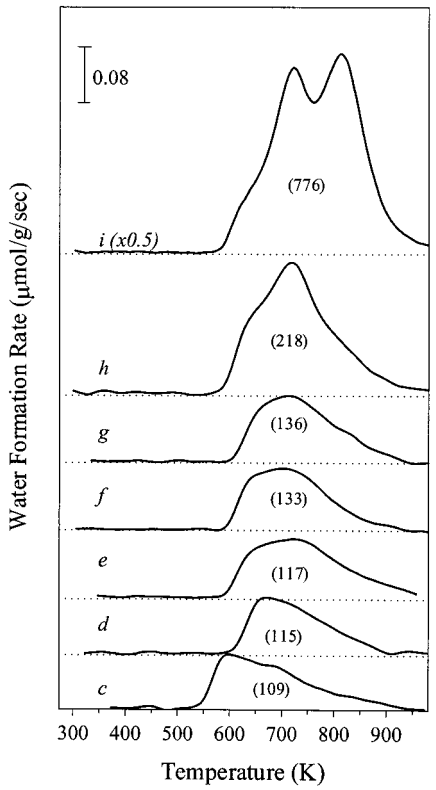

Figure 5. Water evolution in TPO on 4 wt % Mo/H−ZSM5 after methane reaction and D−H exchange. (Letters in the figure follow the meaning of those in Figure 3, figures are amount of water under peaks (μmol/g).)

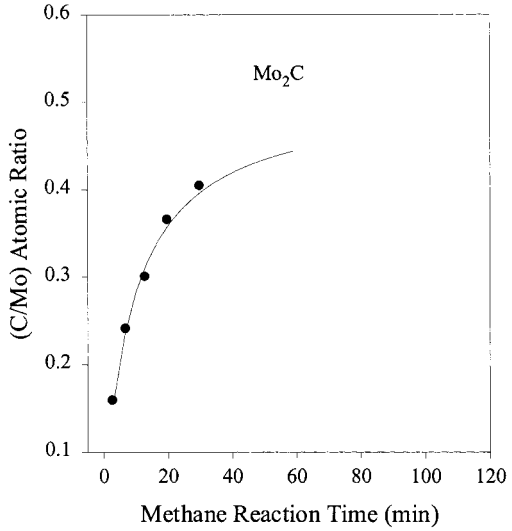

Figure 6. Ratios of Mo with carbon amount under peak 1 of TPO.

the TPO experiments. The H/C ratio after CH_4 reactions at 950 K and H_2 and He treatments also at 950 K decreased from a value greater than 3 at short reaction times to a constant value of ~0.2 for times longer than ~0.3 h. The high initial (H/C) values at short reaction times are atypical of unreactive carbonaceous deposits, which tend to be very hydrogen deficient.[33] One possible mechanism for this apparently high H/C ratio is that small MoC_x clusters initially formed during CH_4 reactions oxidize during TPO and that the resulting MoO_x clusters re-exchange with acidic OH groups to form H_2O via pathways identical to those responsible for the initial anchoring of $(Mo_2O_5)^{2+}$ dimers during their synthesis from MoO_3/H−ZSM5 mixtures. This plausible explanation for the high (H/C) ratio evident during TPO would also imply that these OH groups were re-formed during CH_4 reactions by carburization of these Mo oxo dimers and removal from exchange sites. At longer reaction times, these acid sites may become covered by cationic C_xH_y species, which would compensate the negative charge in the bridging Si−O−Al sites in ZSM5 and act as precursor or spectator species in the observed formation of higher hydrocarbons.[17]

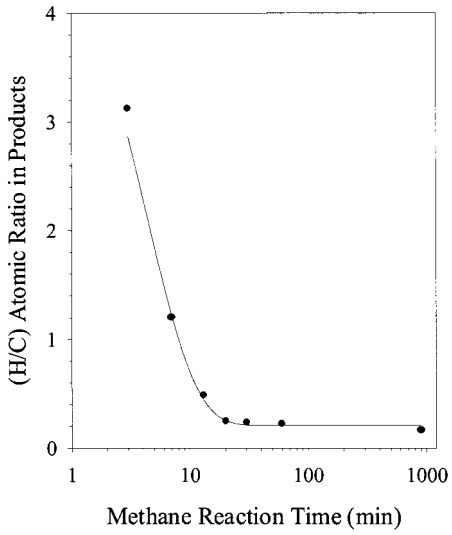

Figure 7. Ratios of hydrogen (H) with carbon under all peaks measured by TPO.

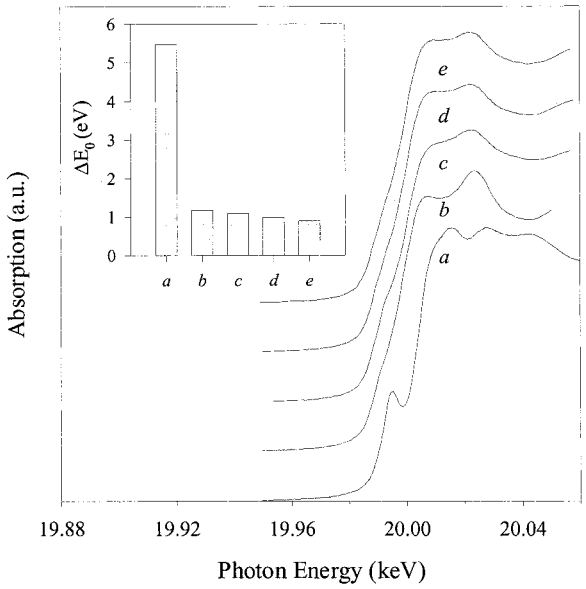

Figure 8. K-edges of molybdenum. (a) physical mixture of MoO_3 with H−ZSM5 heated at 973 K for 0.5 h; (b) in-situ synthesized Mo_2C; (c) 4 wt % Mo/H−ZSM5 reacted with methane at 950 K for 1.33 h; (d) 3.33 h; and (e) 6.33 h. The inset shows the edge shift referenced to molybdenum foil.

Near-edge X-ray absorption spectra for Mo/H−ZSM5 samples treated at various conditions are shown in Figure 8. The Mo−K absorption edges shift to lower energies during CH_4 reaction at 950 K ($\Delta E \approx 5$ eV) and the preedge feature corresponding to Mo(VI) disappears, consistent with the reduction of Mo(VI) centers. The k^3-weighted experimental and simulated molybdenum radial distribution functions are shown in Figure 9 for Mo/H−ZSM5 after reaction with methane for various periods of time. The corresponding results for Mo_2C prepared by carburization of bulk MoO_3[29,30] are also shown in this Figure 9.

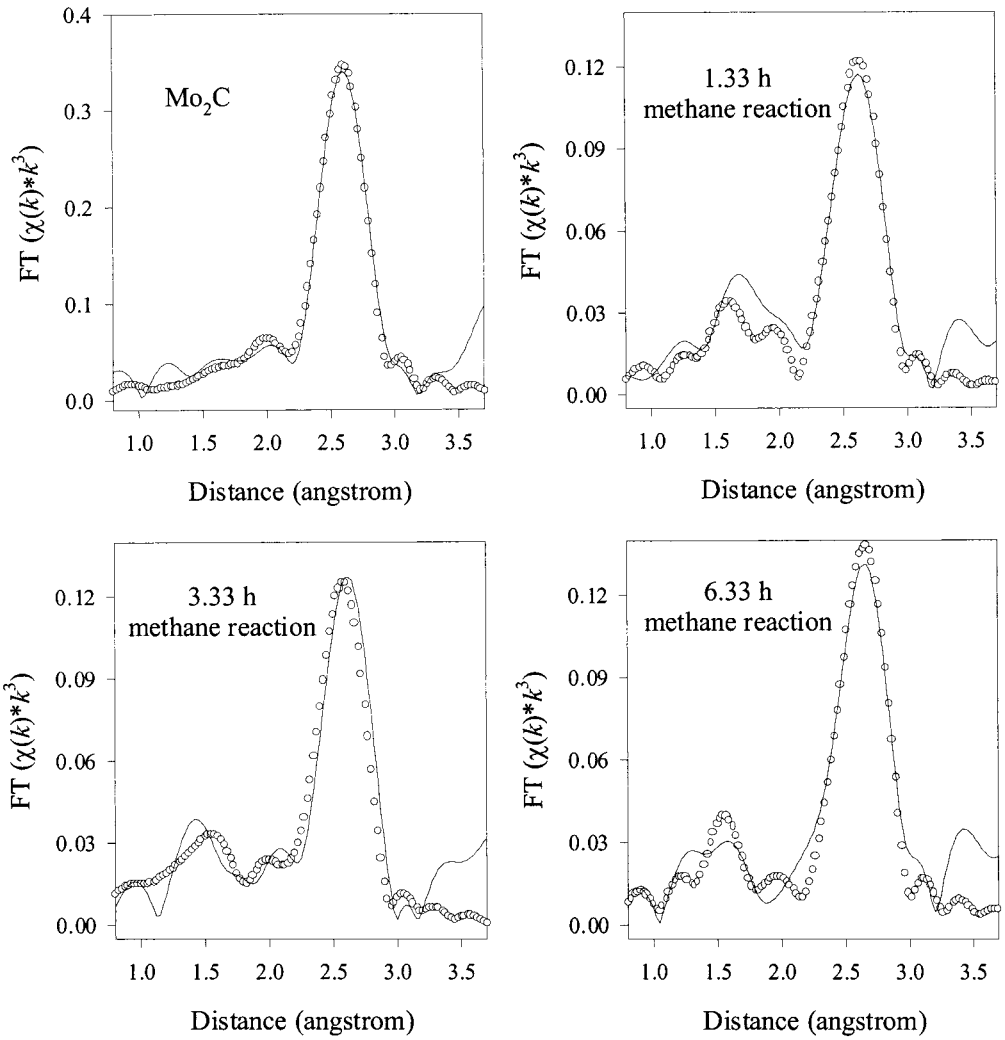

Figure 9. Molybdenum radial distribution functions of Mo_2C and 4 wt % Mo/H−ZSM5 reacted with methane for different times. Lines: experiment data; dots: fit results.

TABLE 1: Mo_2C Structure Parameters Obtained by Analysis of Mo−K−EXAFS

	coordination number		distance (Å)		σ^{2a}
shells	ref (30)	this work	ref (30)	this work	this work
Mo−C (1)	1	1	2.091	2.130	5.4e-5
Mo−C (2)	1	1	2.114	2.137	6.1e-5
Mo−C (3)	1	1	2.118	2.129	7.3e-5
Mo−Mo (4)	1	1	2.898	2.826	4.5e-5
Mo−Mo (5)	1	1	2.900	2.867	6.4e-5
Mo−Mo (6)	2	2	2.936	2.894	4.5e-5
Mo−Mo (7)	1	1	2.975	2.972	3.4e-5
Mo−Mo (8)	1	1	2.977	2.975	7.9e-5
Mo−Mo (9)	4	4	3.009	2.978	7.9e-5
Mo−Mo (10)	2	2	3.013	3.070	3.4e-5

[a] σ^2: Debye−Waller factor.

Before examining the structure of MoC_x species formed during CH_4 reactions on MoO_x/H−ZSM5 precursors, the structure of the bulk Mo_2C prepared from MoO_3 in the XAS cell was examined and compared with previous reports (Table 1). The structure compares well with that reported by Epicier et al.[34] Mo in bulk Mo_2C has three carbon neighbors at a distance of about 0.21 nm and twelve Mo neighbors at distances from 0.290 to 0.301 nm. For the Mo/H−ZSM5 samples reduced and carburized during CH_4 reactions, the Mo K-EXAFS fine structure was fitted using shells between 0.08 and 0.368 nm from the Mo absorber. The structure of Mo_2C (Table 1) was used as the starting point in the structural determination and the structure was refined in order to improve agreement with the experimental radial structure functions. The Mo−C and Mo−Mo coordination numbers, interatomic distances, the Mo−Mo Debye−Waller factors, and energy shifts were allowed to vary in order to describe the experimental results. The Mo−C Debye−Waller factor was held at zero because a strong correlation between the Mo−C coordination number and the corresponding Debye−Waller factor prevented convergence using physically reasonable structural parameters. Although the Mo site in bulk Mo_2C is described by three Mo−C and seven Mo−Mo distances, within what could be broadly regarded as the first two coordination shells, these collapsed into single Mo−C and Mo−Mo distances when the same model was used to fit the EXAFS from the carburized Mo/H−ZSM5 samples. The analysis results, listed in Table 2, show one Mo−C and one Mo−Mo shell are sufficient to describe the radial structure function of the Mo−C species present during CH_4 reactions on Mo/H−ZSM5 catalysts.

The simulated and the experimental radial distribution functions are shown in Figure 9. Mo-C and Mo−Mo interatomic distances were 0.210 and 0.297 nm, respectively. These are similar to those in Mo_2C bulk, implying that the local structures of Mo atoms in Mo_2C and in MoC_x/H−ZSM-5 are very similar. Even after CH_4 reacts for 1.3 h, the Mo−Mo coordination number is close to 3 (Table 2), instead of the value of 12

TABLE 2: MoC_x Structure of 4 wt % Mo/H-ZSM5 in Methane Reaction[a]

	Mo−C shell				Mo−Mo shell			
time on stream (h)	coordination number	distance (Å)	σ^2	ΔE_0	coordination number	distance (Å)	σ^2	ΔE_0
1.3	0.6	2.110	0	−6.1	2.6	2.968	0.004	−6.1
3.3	1.0	2.083	0	−6.6	3.3	2.963	0.006	−6.8
6.3	1.1	2.074	0	−5.4	3.4	2.971	0.005	−5.4

[a] σ^2: Debye−Waller factor.

SCHEME 2. Reaction of Exchanged of MoO_x/H-ZSM5 with CH_4.

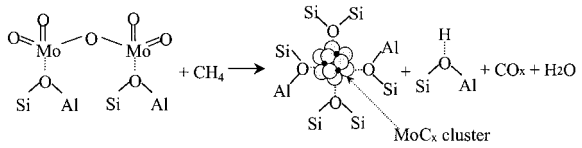

expected for large Mo_2C crystallites, suggesting that isolated Mo precursors form very small Mo_2C clusters during the initial stages of reduction and carburization. The Mo−Mo coordination numbers increased slightly with increasing reaction time, consistent with the subsequent gradual growth of these initial MoC_x clusters during CH_4 reactions. Using an analogy with previously reported effects of cluster size on coordination number for metal particles[35] and the parameters listed in Table 2, we estimate MoC_x clusters to be ∼0.6 nm diameter and to contain ∼10 molybdenum atoms. Perhaps coincidentally, this cluster size is similar to the diameter of the channels in ZSM5 (0.55 × 0.57 nm) within which these MoC_x clusters are likely to reside.

At longer CH_4 reaction times, the size of the MoC_x clusters may exceed the channel diameter. Then, clusters must reside at channel intersections, crystalline defects, or external surfaces. Metal clusters have been shown to migrate readily to external zeolite crystal surfaces at high temperatures. For example, it was reported that Co metal clusters confined within Y zeolite migrate to form large crystallites at external zeolite surfaces at ∼473 K.[36,37] In contrast, MoC_x clusters within ZSM5 channels remain small and unusually resistant to migration and external agglomeration at even higher temperatures. MoC_x nanostructures smaller than ∼1 nm in size are evident during CH_4 reactions at 950 K for several hours. The high melting point and low vapor pressure of molybdenum carbides,[38,39] the high initial dispersion of the MoO_x precursors, and the possible complexation of MoC_x clusters by framework oxygens may contribute to the remarkable structural stability of these MoC_x/H−ZSM5 materials.

These data lead to the pathways for reduction of $(Mo_2O_5)^{2+}$ dimers to form MoC_x clusters shown schematically in Scheme 2. The oligomerization of isolated Mo dimers into small clusters releases the monomers from exchange sites with the concurrent regeneration of the acidic OH groups, initially replaced by $Mo_2O_5^{2+}$ dimers during the synthesis from physical mixtures of MoO_3 and H−ZSM5. The aggregation of molybdenum to form carbide clusters releases most of acid sites required for aromatization reactions of intermediates.

This mechanistic suggestion, in turn, leads us to a description of the initial stages of the reduction and carburization of the precursor MoO_x dimers. C−H bonds in CH_4 are activated slowly until O-atoms start to be removed as CO and H_2O after the initial C−H bond activation step. As oxygen atoms continue to be removed, C−H bond activation becomes more facile and carbidic carbon is gradually deposited. The strong bond between carbidic carbon and molybdenum causes the aggregation of molybdenum to form Mo−C clusters. The depositing of carbidic carbon passivates the surface against further carbon deposition, but still allows the catalytic activation of C−H bonds. The catalytic ability of MoC_x sites in activation of C−H bonds in alkanes has been widely reported, in the context of hydrogenation and dehydrogenation reactions.[30,31]

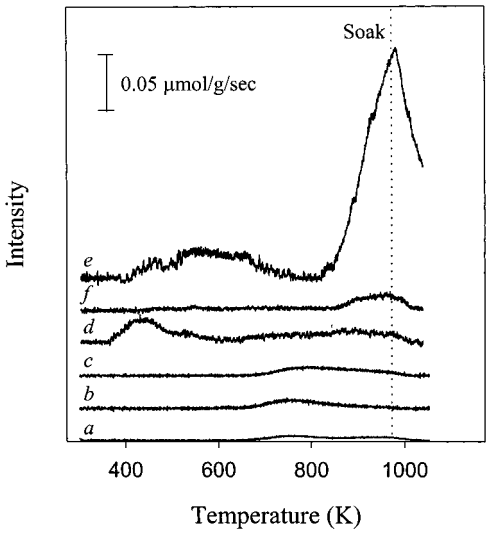

Figure 10. Desorbed species with $m/z = 17$ (curves *a* and *d*), 18 (curves *b* and *e*), and 19 (curves *c* and *f*) during temperature-programmed D_2/Ar treatment on methane reacted 4 wt % Mo/H−ZSM5 followed by hydrogen (curves *a*, *b*, and *c*) or helium (curves *d*, *e*, and *f*) treatment.

One important and challenging question remaining in this mechanistic proposal is the nature of the intermediates involved in the formation of C−C bonds from CH_x fragments formed by C−H bond activation in CH_4. We have attempted to probe this quenching of the CH_4 reaction and attempting the deuteriogenation of any CH_x present using D_2.

Figure 10 shows the rates of desorption of species with masses 17, 18, and 19 amu during deuterogenation experiments as a function of temperature during reactions of D_2 with H-species present in Mo/H−ZSM5 after CH_4 reactions. The mass fragments detected correspond to the parent ions for CH_3D, CH_2D_2 and CHD_3, respectively. The various profiles shown in Figure 10 correspond to samples treated by procedures (*a*) to (*f*) (see Methods section), but without the H_2 treatment of step (*e*) for curves *d* ∼ *f* in Figure 10. This last step was avoided in an attempt to preserve, to the extent possible, the density and type of methane-derived intermediates present during reaction. These data were obtained after methane reactions were carried out for a period of time (1 h) sufficient to ensure the complete reduction and carburization of the MoO_x precursors. The results obtained on the same catalyst, but after a H_2 treatment using the procedure described in step (*e*), are also given in the Figure 10 for comparison. An accurate measurement of the concentration of the various methane isotopomers is difficult because of significant kinetic isotopic effects in the fragmentation of $CH_{4-x}D_x$ isotopomers and because of the strong overlap among the mass

spectra from the various isomers. Qualitatively, these data reflect, however, the relative surface concentrations of CH_x fragments formed from methane during steady-state catalysis. CH_2 appears to be the most abundant surface fragment present during methane reactions, whereas CH_3 fragments are less abundant but react with D_2 at a lower temperature. CH fragments are lowest in abundance. The temperature required for the reactive desorption of CH_3 to form CH_3D is ~450 K, which is lower than for the reaction of CH_2 to form CH_2D_2. This mainly reflects the different adsorption strength of CH_3 and CH_2 and not necessarily the relative kinetic importance of these two possible intermediates during methane reactions.

Solymosi et al. have detected the presence and conversion to adsorbed CH_2 of CH_3 formed from CH_3I on the surface of Mo_2C grown on Mo (111) using TPD and EELS (electron energy loss spectroscopy).[40] They observed the desorption of CH_4 at ~300 K and C_2H_4 at ~520 K after adsorption of CH_3I at 100 or 300 K. Their results suggest that CH_3 and CH_2 species adsorbed on Mo_2C are stable. It is reasonable to expect stronger interactions of CH_x fragments with nanoclusters of molybdenum carbides than with bulk carbide surfaces because of higher coordinative unsaturation of Mo centers in such small clusters. As a result, it is likely that these CH_x fragments condense on the surface of Mo−C clusters to form C_2H_4 or C_2H_6 molecules, which can oligomerize and cyclize to form aromatics on Brönsted acid sites aided by the presence of MoC_x species that desorb hydrogen as H_2 during methane reactions.[19]

Conclusions

The reduction and carburization of $(Mo_2O_5)^{2+}$ species during CH_4 reactions cause the formation of MoC_x clusters (0.6−1 nm diameter) and the concurrent regeneration of the bridging OH groups initially displaced by the Mo oxo dimers during catalyst synthesis. In this manner, MoO_x species initially exchanged but catalytically inactive convert into the two catalytic functions required for CH_4 conversion: MoC_x for C−H bond activation and C_2 formation and Brönsted acid sites for the formation of aromatics from C_2. These MoC_x clusters contain ~10 Mo atoms and they resist agglomeration for extended times (~10 h) during methane reactions at 950 K. C−H bond activation on these clusters lead to the formation of CH_x species that condense to give the initial C_2 products of methane conversion reactions.

Acknowledgment. This work has been supported by the Division of Fossil Energy of the U.S. Department of Energy (Contract No. DE-AC03-76SF00098) under the technical supervision of Dr. Daniel Driscoll. The authors gratefully acknowledge the Stanford Synchrotron Radiation Laboratory for all the measurements of X-ray absorption spectroscopy included in this paper. W.D. thanks Nanjing University for his leave of absence to work at the University of California at Berkeley.

References and Notes

(1) Guczi, L.; VanSanten, R. A.; Sarma, K. V. *Catal. Rev.* **1996**, *38*, 249.
(2) Eng, D.; Stoukides, M. *Catal. Rev.* **1991**, *33*, 375.
(3) Fox, J. M. *Catal. Rev.* **1993**, *35*, 169.
(4) Xu, Y. D.; Lin, L. W. *Appl. Catal., A* **1999**, *188*, 53.
(5) Wang, L. S.; Tao, L. X.; Xie, M. S.; Xu, G. F.; Huang, J. S.; Xu, Y. D. *Catal. Lett.* **1993**, *21*, 35
(6) Weckhuysen, B. M.; Wang, D. J.; Roseynek, M. P.; Lunsford, J. H. *J Catal.* **1998**, *175*, 338.
(7) Zhang, C. L.; Li, S.; Yuan, Y.; Zhang, W.; Wu, T.; Lin, L. W. *Catal. Lett.* **1998**, *56*, 207.
(8) Liu, S. T.; Wang, L. S.; Ohnishi, R.; Ichikawa, M. *J Catal.* **1999**, *181*, 175.
(9) Xu, Y. D.; Liu, S. T.; Wang, L. S.; Xie, M. S.; Guo, X. X. *Catal. Lett.* **1995**, *30*, 135.
(10) Shu, Y. Y.; Xu, Y. D.; Wong, S. T.; Wang, L. S.; Guo, X. X. *J. Catal*. **1997**, *170*, 11.
(11) Chen, L. Y.; Lin, L. W.; Xu, Z.; Li, X.; Zhang, T. *J. Catal.* **1995**, *157*, 190.
(12) Wang, D. J.; Lunsford, J. H.; Rosynek, M. P. *J. Catal.* **1997**, *169*, 347.
(13) Solymosi, F.; Szöke, A. *Appl. Catal., A* **1998**, *166*, 225.
(14) Solymosi, F.; Erdohelyi, A.; Szöke, A. *Catal Lett.* **1995**, *32*, 43.
(15) Solymosi, F.; Szöke, A. *Appl. Catal., A* **1996**, *142*, 361
(16) Solymosi, F.; Cserenyi, J.; Szöke, A.; Bansagi, T.; Oszko, A. *J. Catal.* **1997**, *165*, 150.
(17) Wang, D. J.; Lunsford, J. H.; Rosynek, M. P. *Top. Catal.* **1996**, *3*, 289.
(18) Li, W.; Meitzner, G. D.; Borry, R. W.; Iglesia, E. *J. Catal.* **2000**, *191*, 373.
(19) Borry, R. W.; Kim, Y. H.; Huffsmith, A.; Reimer, J. A.; Iglesia, E. *J. Phys. Chem. B* **1999**, *103*, 5787.
(20) Borry, R. W.; Lu, E. C.; Kim, Y. H.; Iglesia, E. *Stud. Surf. Sci. Catal.* **1998**, *119*, 403.
(21) Kim, Y. H.; Borry, R. W.; Iglesia, E. *J Ind. Eng. Chem.* **2000**, *6*, 72.
(22) (a) Meitzner, G.; Iglesia, E. *Catal. Today* **1999**, *53*, 433. (b) Barton, D. G.; Soled, S. L.; Meitzner, G. D.; Fuentes, G. A.; Iglesia, E. *J. Catal.* **1999**, *181*, 57.
(23) Lee, J. S.; Oyama, S. T.; Boudart, M. *J. Catal.* **1987**, *106*, 125.
(24) WinXAS97 is an XAS data analysis program for PCs running MS Windows by Thorsten Ressler (e-mail: t_ressler@compuserve.com; webpage: http://ourworld.compuserve.com/homepages/t_ressler).
(25) Rehr, J. J.; Albers, R. C.; Zabinsky, S. I. *Phys. Rev. Lett.* **1992**, *69*, 3397.
(26) The code ATOMS is written by Bruce Ravel (e-mail: ravel@u.washington.edu) to calculate coordination numbers and interatomic distances from compounds with known structures and all input for FEFF8.0.
(27) Borry, R. W, Ph.D. Dissertation, University of California at Berkeley, USA, 1998.
(28) Arnold, P.; de Jonge, J. C. M.; Moulijn, J. A. *J. Phys. Chem.* **1985**, *89*, 4517.
(29) Lee, J. S.; Volpe, L.; Ribeiro, F. H.; Boudart, M. *J. Catal.* **1988**, *112*, 44.
(30) Lee, J. S.; Locatelli, S.; Oyama, S. T.; Boudart, M. *J. Catal.* **1990**, 125, 157
(31) Lee, J. S.; Boudart, M.; *Catal. Lett.* **1993**, *20*, 97.
(32) Oyama, S. T. *Catal. Today* **1992**, *15* (2), 179.
(33) Kim, Y. H.; Borry, R. W.; Iglesia, E. *Micropor. Mesopor. Mat*. **2000**, *35*, 495.
(34) Epicier, T.; Dubois, J.; Esnouf, C.; Fantozzi, G.; Convert, P. *Acta Metall.* **1988**, *36*, 1903.
(35) Feeley, O.; Sachtler, W. M. H. *Appl. Catal.* **1990**, *67*, 141.
(36) Zhang, Z.; Zhang, Y. D.; Hines, W. A.; Budnick, J. I.; Sachtler, W. M. H. *J. Am. Chem. Soc.* **1992**, *114*, 4843.
(37) Ryoo, R.; Cho, S. J.; Pak, C. H.; et al. *J. Am. Chem. Soc.* **1992**, *114*, 76.
(38) Suzuki, Y.; Niihara, K. *Intermetallics* **1998**, *6*, 7.
(39) King, H. W.; Pho, I. *Can. Ceram. Quart.* **1997**, *66*, 136.
(40) Solymosi, F.; Bugyi, L.; Oszko, A. *Catal. Lett.* **1999**, *57*, 103.